National Aeronautics and Space Administration
Goddard Space Flight Center
Contract No.NAS-5-12487

ST-AM-SPC-10649

THE SPECTRAL COMPOSITION OF THE EARTH'S INFRARED RADIATION INTO SPACE ACCORDING TO THE MEASUREMENT RESULTS FROM EARTH'S ARTIFICIAL SATELLITES

by

A. I. Lebedinskiy
Yu. G. Andranov
G. N. Barkova
.... ET AL .....

(USSR)

4 OCTOBER 1967

ST-AM-SPC-10649

THE SPECTRAL COMPOSITION OF THE EARTH'S INFRARED RADIATION INTO SPACE ACCORDING TO THE MEASUREMENT RESULTS FROM EARTH'S ARTIFICIAL SATELLITES

*

Paper read by A. I. Lebedinskiy
at the X COSPAR ASSEMBLY
LONDON, ENGLAND, July 1967

by A. I. lebedinskiy
Yu. G. Andrianov
G. N. Barkova
... ET AL .....

ABSTRACT

The spectra of outgoing radiation were measured in the 7-38μ range using satellite-borne monochrmomators. Up to 10,000 spectra were thus obtained. It took 20 seconds to obtain each spectrum, the resolution on the ground being 10 km.

The measured spectra were selectively compared with those computed from the data of aerological sounding. To that effect the spectra selected were those obtained during the flight at meteorological stations at times close to the dates of aerological soundings.

The near-ground temperatures were selectively compared with the temperatures for various wavelengths measured from the satellite in cloudless regions. The connection was analyzed of the spatial distribution of radiation temperatures for various wavelengths with the distribution of cloudiness along orbits. A statistical processing of 1278 spectrograms was made for the Earth as a whole without breaking them up into latitude ranges. The unidimensional differential laws of distribution, i. e., the densities of probability of spectral intensity of the outgoing radiation have been approximated using the Pearson's curves. The correlation factors for the spectral intensity of the outgoing radiation in various spectral ranges are determined on the basis of the analysis of the two-dimensional differential laws of distribution.

The effective temperatures of radiation at various points of our planet in the 8-13 μ range are very different, but beyond the longwave boundary of the CO_2 bands in the 19-26 μ wavelength range these temperatures are constrained within the narrow range of about 10°C order.

---

* From revised and improved preprint

*
* *

Some of the Soviet artificial Earth's satellites of the "Cosmos" series were provided with diffraction grating spectrophotometers [1], with the aid of which a large number of spectrograms of the outgoing radiation were obtained in the 7 ÷ 38μ spectral range.

The instruments' optical axes were oriented along the local vertical. The devices measured the intensity of the radiation from a site of the Earth's surface of 7 by 10 km dimension at the average flight altitude of about 250 km.

Presented below are the results of processing of a portion of the obtained information using both the statistical method and that of the analysis of satellite measurements and the data from the ground meteorological network.

The statistical treatment of the observation material consisted in plotting the curves of radiation intensity distribution in various spectral ranges and also in determining the correlations between the values of these intensities. In accord with the spectral resolution of the instrument, the spectrum was broken into 1μ and 2μ intervals respectively in the 7 – 15μ and 14 – 26μ ranges. This 1176 spectrograms in the 7 – 15μ range and 1287 spectrograms in the 14 – 26μ range were utilized, which amounted to about one half of the total of "COSMOS-45" measurements.

Fig.1 presents the results bearing on the distribution of Earth's radiation intensity in various spectral ranges. Plotted in the abscissa are the values of $\underline{x}$ (radiation intensity in a specific spectral range), and in ordinates — the density of the probability f(x).

The cases of overshoots of the processes observed on the film in the 10 – 11 and 11 – 12μ spectral ranges amounted to six percent (6%) of the total of the recorded events ; in the 9 – 10μ range such cases amounted to four percent (4%). When treating these cases, they were ascribed to the last interval of Δx.

Plotted in the same Fig.1 are the Pearson curves [2], which smooth out the obtained experimental statistical distributions. Two types of Pearson equations were used for these flattenings:

$$f(x) = y_0 \left(1 + \left(\frac{x - M}{A_1}\right)^{M_1}\right)\left(1 - \left(\frac{x - M}{A_2}\right)^{M_2}\right) \qquad (1)$$

$$f(x) = y \left[1 + \frac{(x - A_2)^2}{A_1^2}\right]^{-M_1} e^{-M \operatorname{arc\,tg} \frac{x - A_2}{A_1}} \qquad (2)$$

The numerical coefficients in Eqs.(1) and (2), calculated for the distribution in all spectral ranges, are compiled in Table 1.

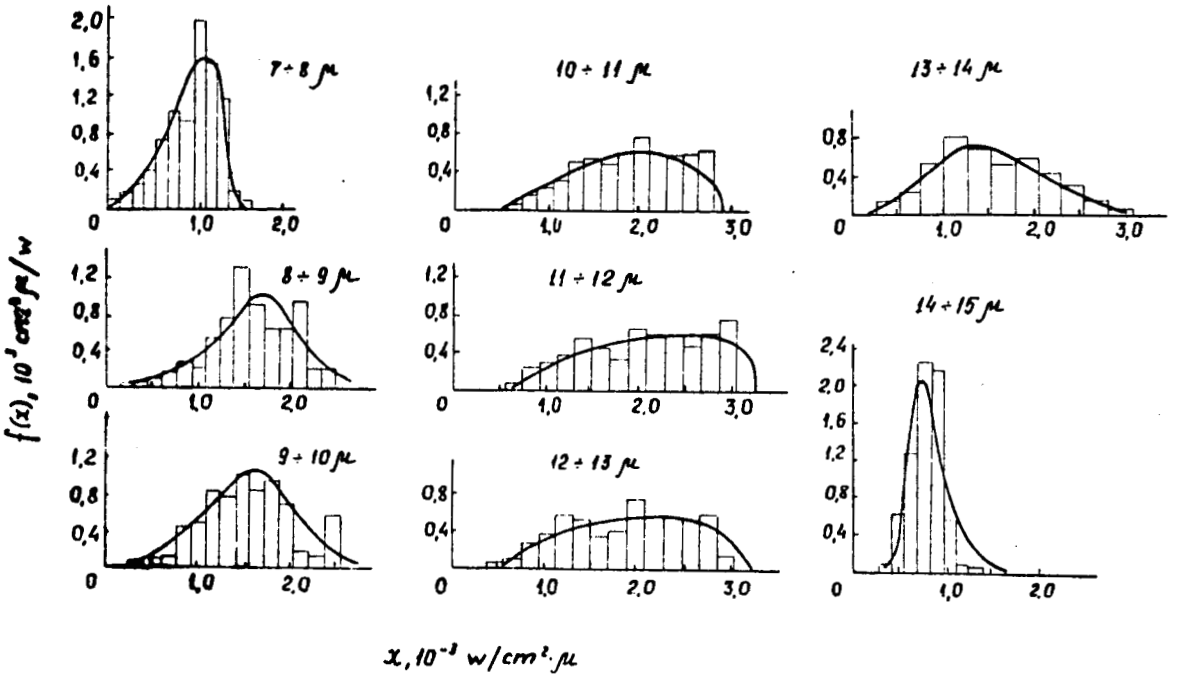
7 ÷ 8 μ
10 ÷ 11 μ
13 ÷ 14 μ
8 ÷ 9 μ
11 ÷ 12 μ
14 ÷ 15 μ
9 ÷ 10 μ
12 ÷ 13 μ
f(x), 10⁻³ cm²μ/w
x, 10⁻³ w/cm².μ

Fig.1a

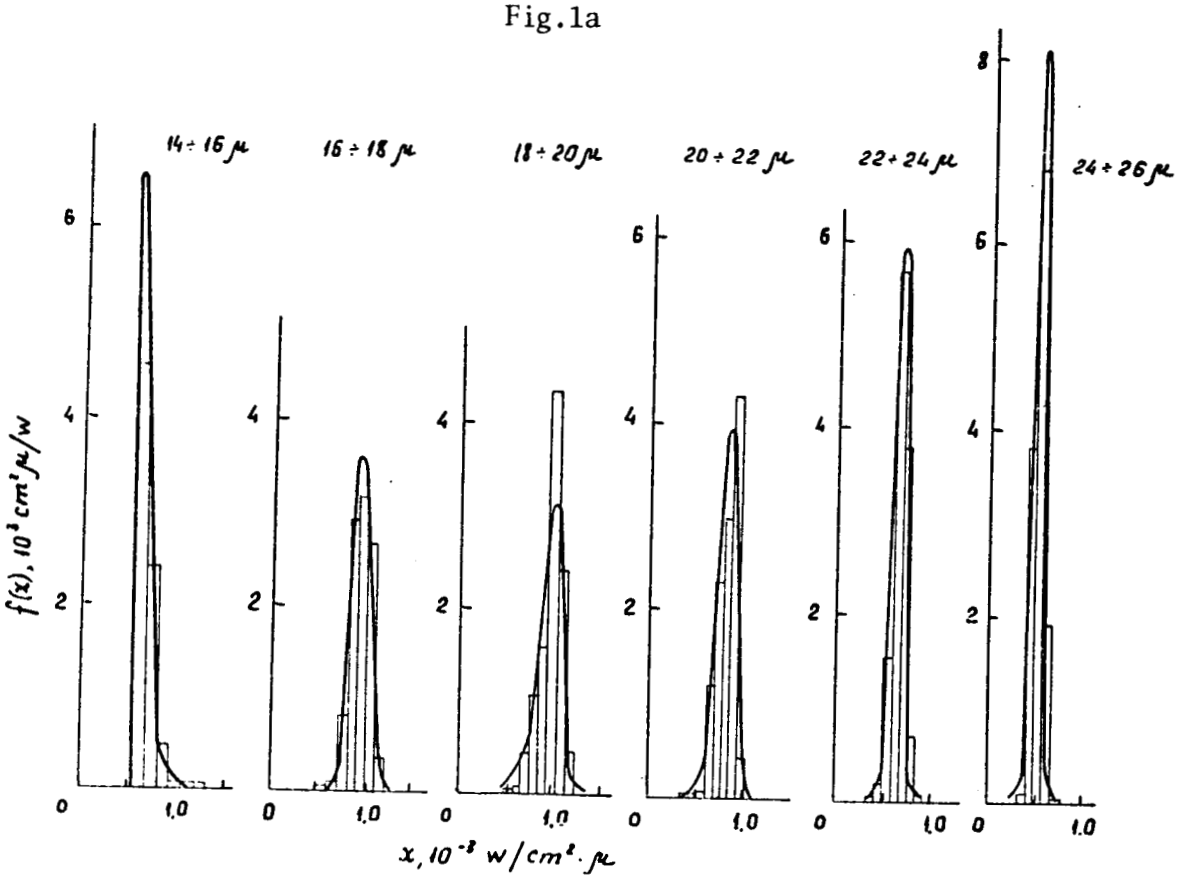
14 ÷ 16 μ
16 ÷ 18 μ
18 ÷ 20 μ
20 ÷ 22 μ
22 ÷ 24 μ
24 ÷ 26 μ
f(x), 10⁻³ cm²μ/w
x, 10⁻³ w/cm².μ

Fig.1b

Table 1

spectral ranges μ	M, $10^{-3}\ \frac{w}{cm^2 \mu}$	y_o, $10^3\ \frac{cm^2 \mu}{w}$	M_1	M_2	A_1 $10^{-3}\ \frac{w}{cm^2 \mu}$	A_2 $10^{-3}\ \frac{w}{cm^2 \mu}$
7 - 8	I,0	I,59	6,09	I,3I	I,57	0,34
8 - 9	I,69	0,99	I76,0	I4,30	I9,60	I,59
9 - I0	I,53	0,99	46,7	7I,80	3,90	6,02
I0 - II	2,I0	0,62	I,I6	0,57	I,62	0,80
II - I2	2,77	0,55	0,68	0,I3	2,I0	0,42
I2 - I3	2,23	0,53	0,52	0,23	I,66	0,72
I3 - I4	I,32	0,7I	3,06	6,94	I,25	2,83
I4 - I5	0,75	0,I8	2,98	-5,76	0,28	0,47
I4 - I6	0,59	6,64	0,24	I5,70	0,023	I,52
I6 - I8	0,95	3,60	I3,40	7,04	0,7I	0,37
I8 - 20	I,02	$0{,}48.I0^{-4}$	7,I5	I9,8I	0,26	I,39
20 - 22	0,88	3,94	I3,I0	2,38	0,93	0,I7
22 - 24	0,66	4,56	5,74	2,45	0,2I	0,70
24 - 26	0,52	6,85	3,48	I,56	0,II	0,54

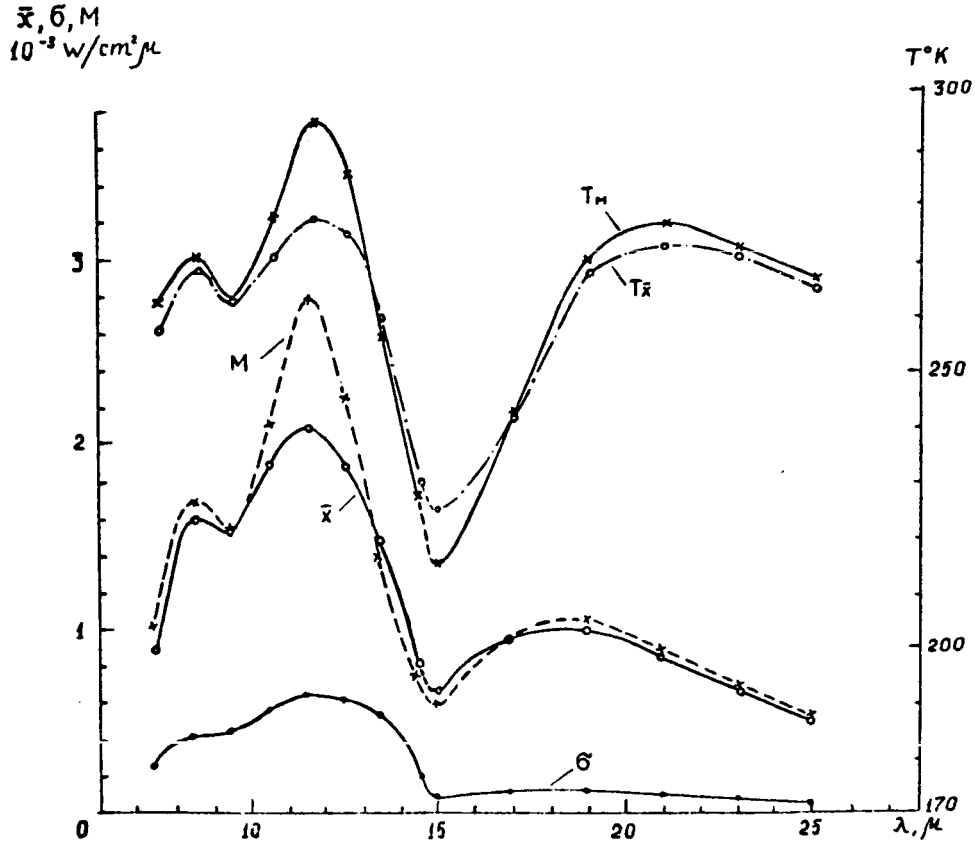

Fig.2

Eq.(1) was used for the majority of spectral ranges and Eq.(2) — for the 14 ÷ 15, 18 ÷ 20, 22 ÷ 24 and 24 ÷ 25μ ranges.

Fig.2 shows the numeiical characteristics of the obtained statistical distributions as a function of the wavelength , $\bar{x}$ is the mathematical expectation, M is the mode, σ is the mean root deviation (left scale). Besides, Fig.2 presents the dependence of the effective temperature of the absolute blackbody corresponding to the Earth's radiation intensity; $T_{\bar{x}}$ is the temperature found from the mathematical expectation of the intensity; T_M is that found from the mode (the right scale).

The above distribution laws of radiation intensities are global, i. e., they reflect the character of the Earth's radiation as a whole, without dividing it into ensembles (sunlit and dark sides, cloud and cloudless conditions, land and sea, geographical coordinates etc.). The latitude dependence of radiation intensity is presented in Fig.3 for various spectral ranges.

It follows from the results obtained that the minima of radiation intensity (minima of the values of $\bar{x}$ and M) are narrow laws of intensity distribution, i. e., the minima of intensity fluctuations (minima of the values of σ) correspond to the bands of atmospheric gas absorption (9.6μ for ozone and 15μ for carbon dioxide). The intensity distribution is broadest in the transparency "window" of the Earth's atmosphere (8 ÷ 12μ) and the distribution function is close to the law of equal density.

The distribution of radiation intensity in the 14 ÷ 26μ spectral range has a small scatter with respect to the amplitude and a weak latitude dependence. In the 18 ÷ 26μ spectral range the temperature $T_{\bar{x}}$ is within the 265 - 272° range and T_M is within 267 - 276° K.

Hence the spectrum of the outgoing radiation in this wavelength range is on the average close to the spectrum of the absolute blackbody with temperature of about 268°.

For the study of radiation intensities' correlation dependences in different spectral ranges the two-dimensional laws of Earth's radiation intensity distributions have been plotted for all combinations of spectral ranges.

As an example, Fig.4 presents the two-dimensional distributions for the spectral ranges corresponding to two bands of weak water vapor absorption (8 ÷ 9μ and 10 ÷ 11μ), as well as to the bands of weak absorption of water vapor and strong absorption of carbon dioxide (11 ÷ 12μ and 14 ÷ 15μ). The numerals inside each square of the grid in Fig. 4 denote the number of the event when the radiation intensities in both spectral ranges discussed has a magnitude limited by the values of the respective sides of the square. The dotted lines in Fig.4 are the plots ff the dependences linking the intensities of radiation of the absolute blackbody in wavelengths corresponding to the centers of the spectral ranges examined. The circles on the curves denote the radiation intensities of the absolute blackbody with temperatures from 200 to 300°K inaccretions of 20°K.

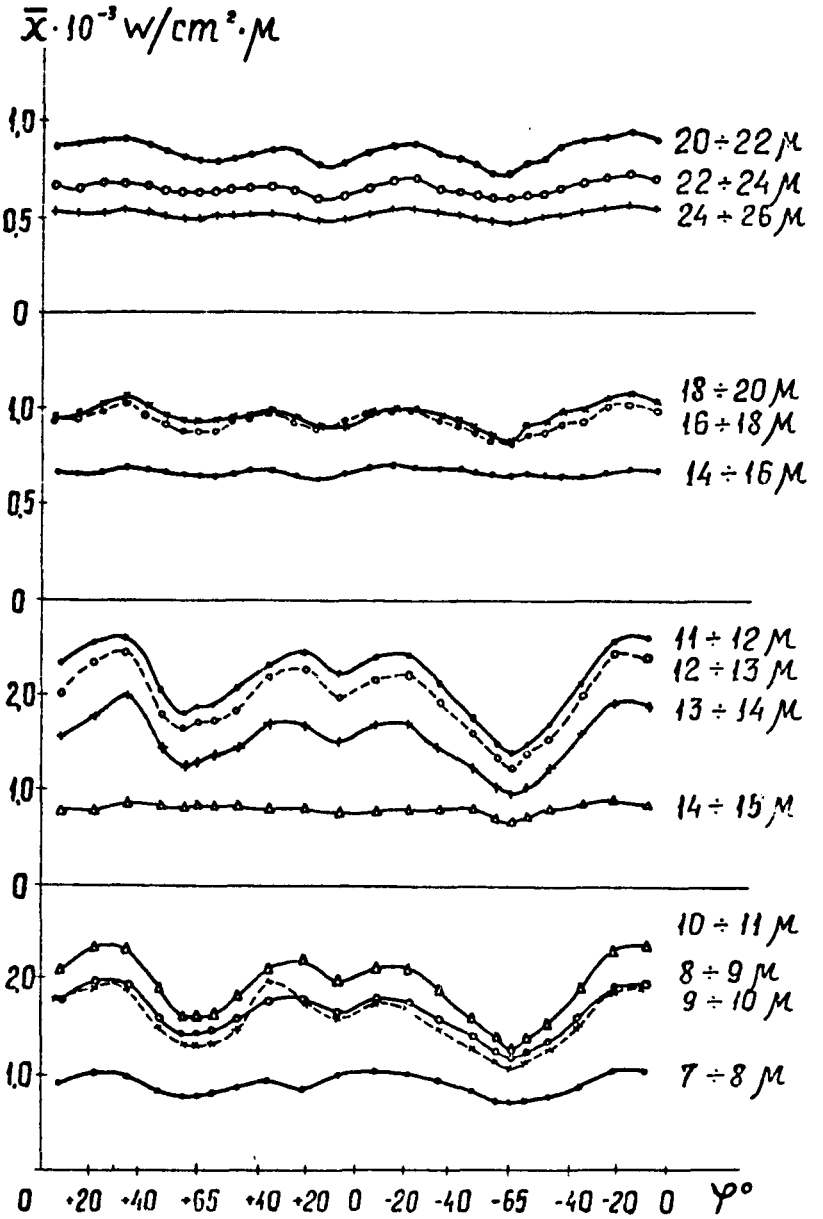

Fig 3

Table 2.

spectral ranges, μ		$K_{x_1 x_2}$	r	$\bar{x}_1$	$\bar{x}_2$	σ_1	σ_2	θ_1
in x - direction (x_1)	in y- direction (x_2)	10^{-6} w^2/cm^4·μ^2		10^{-3} w/cm^2·μ	10^{-3} w/cm^2·μ	10^{-3} w/cm^2·μ	10^{-3} w/cm^2·μ	
8–9	10–11	0.205	0.91	1.60	1.87	0.412	0.548	53.8°
11–12	14–15	0.0476	0.37	2.07	0.792	0.633	0.202	97.4°

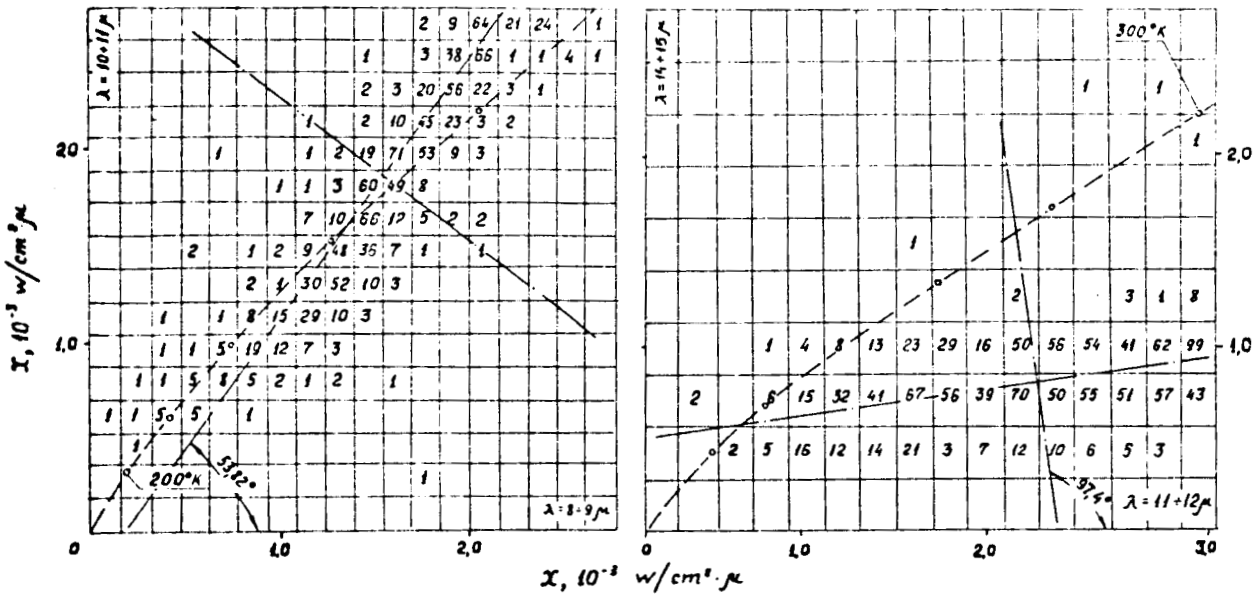

Fig 4

Table 3

WAVELENGTH, λ, μ	$\delta_1 = T_{cal} - T_{meas.}$ °C	$\delta_2 = T_{cal.} - T_{meas}$, °C
8	- 9.9	10.3
9	+ 2.9	4.4
9.5	+ 5.9	5.9
10	+ 4.3	4.9
11	+ 1.6	4.4
12	- 1.0	4.7
13	- 2.2	5.1
14	+ 2.3	4.0
14.5	+10.0	11.6

Table 4

$T_{rad} - T_{air}$	Δ_1	Δ_2
- 15 + - 11	0	9.5
- 10 + - 6	13.0	44.0
- 5 + - 1	29.5	42.0
0 + + 4	41.0	4.5
+ 5 + + 9	13.5	0
+ 10 + + 14	3.0	0

The correlation momenta K, the correlation factors $\underline{r}$, the inclination angle of the main axis of scattering θ_1, as well as the mathematical expectations x_1, x_2 and the mean root deviations σ_1, σ_2 have been computed for the obtained two-dimensional laws of intensity distributions. The values of these numerical characteristics for both examples of Fig.4 are compiled in Table 2. The main axes of scattering are shown as the dash-dotted lines in Fig.4.

The data obtained are evidence that the strong correlation link is between the radiation intensities, the absorption bands of the same atmospheric gas for 8 ÷ 9μ and 10 ÷ 11μ , and that the correlation link between the radiation intensities in the bands of different gases (water vapor and carbon dioxide) is weak.

Simultaneously with the above statistical processing of the observation material the spectra of outgoing radiation measured from COSMOS satellites were compared with the corresponding time and location data of ground meteorological observations and with the data resulting from calculations of radiation in various spectral ranges.

We shall consider, first of all, the problem of agreement with calculation data. The methods of such calculations were described in [3], where some results have also been given of the comparison of spectra in the 8 ÷ 15μ range measured on COSMOS-45 with the calculated ones. Here we shall discuss the similar results in the 8 ÷ 35μ spectral range. Compared again were the spectra measured from the satellite near the stations of aerological soundings at moments of time close to the synoptical dates. First of all comparison was made for stable cloudless conditions.

Sufficiently typical examples of such a comparison are illustrated in Fig.5. It may be seen that the degree of agreement of measured and calculated radiation temperature is strikingly different for the various spectral ranges. The mean differences between the calculated and measured radiation temperatures for some wavelenths (taking into account the sign and with respect to modulus) are compiled, for example, in Table 3. These differences are especially great in the absorption bands, but they are smaller in the transparent spectral ranges.

The differences in the absorption bands are systematic, which is confirmed by the closeness of the values δ_1 and δ_2 to one another. The difference between the calculated and measured may stem from the fact that the scheme for calculating the radiation [3] fails to describe quite correctly the true process of radiation transfer in the atmosphere for spectral ranges related to absorption bands.

It is possible, however, that the absence of sufficiently detailed and accurate information on ozone and CO_2 distribution and on the stratification of temperature and humidity in the stratosphere, is the cause of the difference.

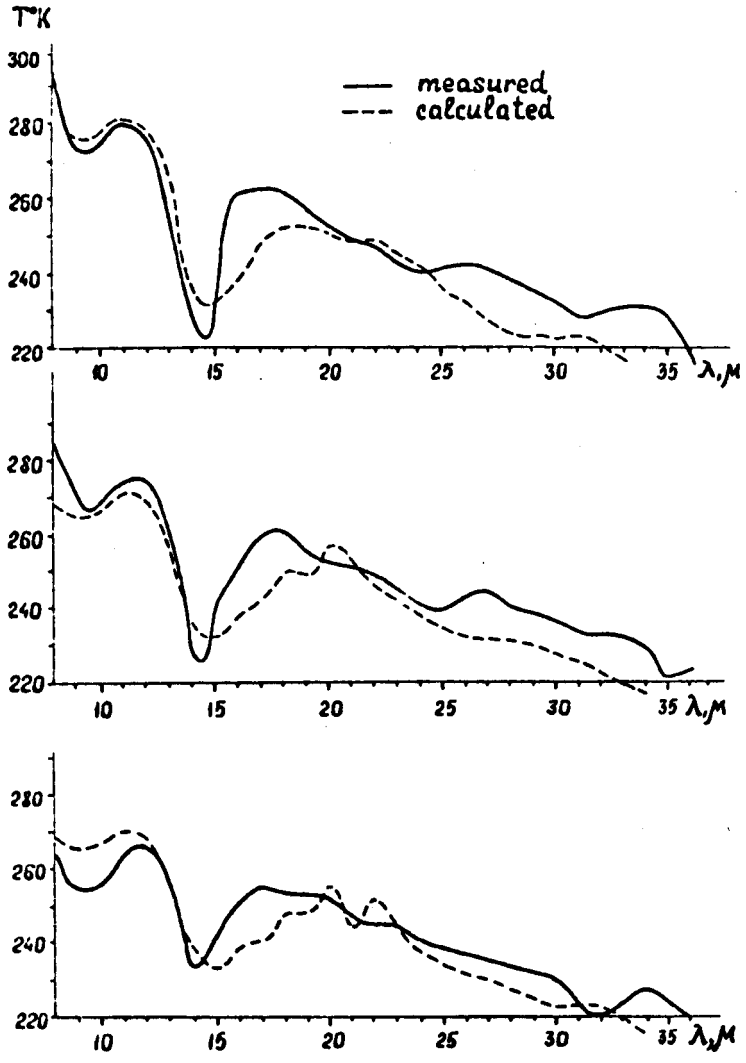

Fig 5

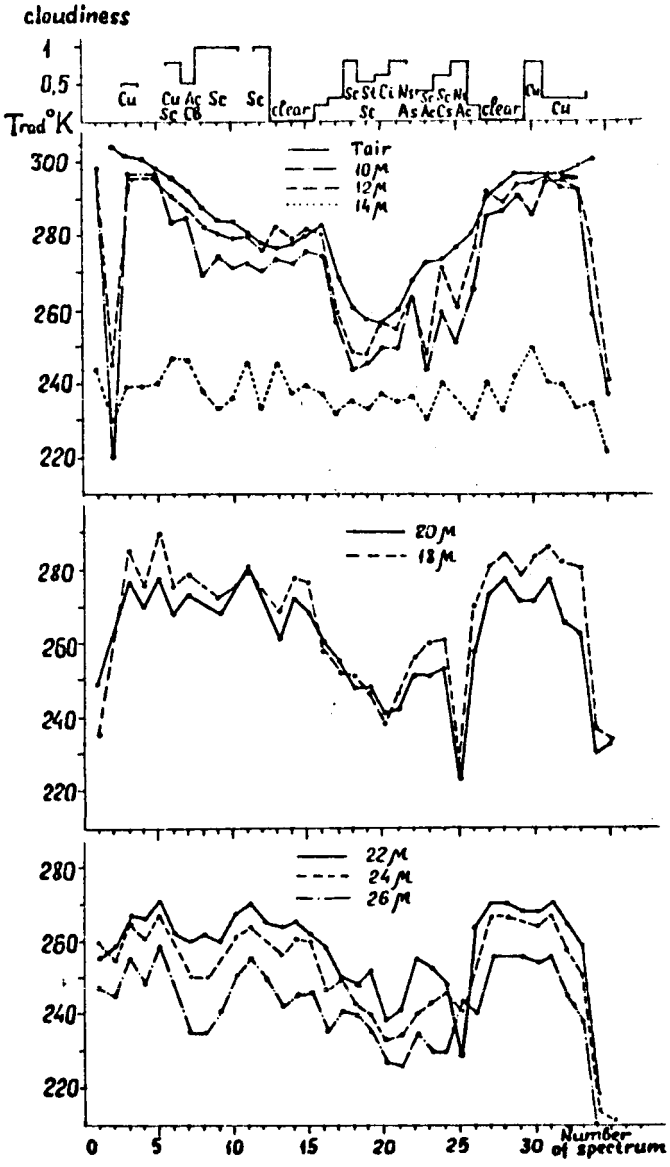

Fig 6

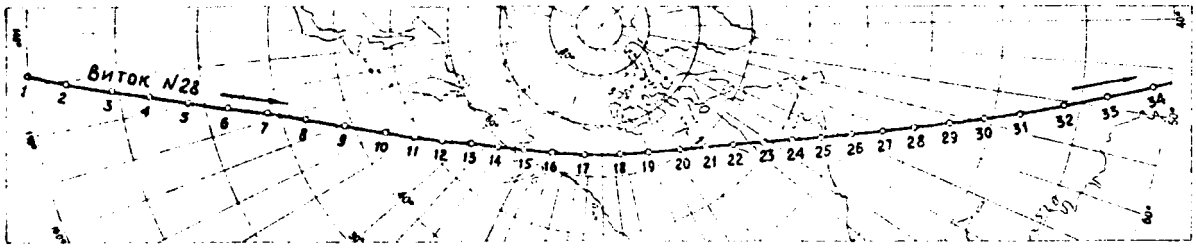

Fig 7

We shall now consider the problem of connection of radiation temperatures of outgoing radiation in various spectral ranges with the distribution of cloudiness and temperatures at various atmospheric levels.

To that effect we plotted the distributions of temperature and cloudiness along orbit trajectories on the basis of cloudiness charts and isotherms at various levels. At the same time the distribution of radiation temperatures was plotted for various wavelengths. The radiation temperatures in the 8 ÷ 15μ and 15 – 35μ ranges were borrowed from the measurements [1] of respectively the shortwave and longwave spectra.

Examples of distributions of cloudiness, near-ground and radiation temperatures for some wavelengths along the orbit trajectory (orbit 28 of COSMOS-65 on April 19, 1965 at about 0300 hours Moscow time) are shown in Figure 6. The orbit in question is illustrated in Fig.7. The numbers of the spectra corresponding to the numbers in the abscissa of Fig.6 are shown along the trajectory. Besides, Fig.6 shows the main types of clouds which were present in the region.

The information on cloudiness in some localities was completely absent and only the amount of clouds without specification of the type was known for other localities. This refers more particularly to the near-equatorial regions. It is nevertheless possible to get a general idea about the cloudiness distribution.

In the case under consideration the main cloud masses were located over No.Canada from a point with 65° N.latitiude and 130° W. longitude up to the eastern coast of North America. Substantial and complete cloud forms with stratocumuli, also-cumuli and stratonimbi were observed. The cirrus and cirrostratus clouds were also absent.

Strato-cumulus clouds were mainly observed over the Pacific, while cloudless conditions prevailed over North American coast in Alaska and the Aleutian island regions. In the Atlantic the satellite orbit crossed mainly cloudless regions and in the tropical regions it crossed localities with cumulus clouds.

The above described features of cloudiness distribution are reflected in the distribution of radiation temperatures, as is shown in Figure 6. Naturally, these features are most pronounced for the distribution of radiation temperature in 8 ÷ 12μ "transparency window".

In the cloudless or little cloudy regions the radiation temperatures in the "transparency window" are close to near-ground temperatures of the air. The values ond the distribution of deviation of radiation temperatures from the near-ground one are quantitatively illustrated in Table 4, where the recurrences of the differences are given:

$$\Delta_1 = T_{rad}(12\mu) - T_{air} \quad \text{и} \quad \Delta_2 = T_{rad}(10\mu) - T_{air}$$

It is of interest to note that the field of cloudiness affects the radiation to a smaller or greater extent practically in all spectral ranges beyond the "transparency window" as well. This refers especially to the 17 ÷ 20μ spectral range. The character of radiation temperature distribution in this spectral range is similar to the temperature distribution in the 8 ÷ 12μ range. In the 17 ÷ 20μ range (with peak at 18 ÷ 19μ), the temperature themselves are 5 to 7° lower than those in the 8 ÷ 12μ range in cloudless regions.

In cloudy regions this difference decreases down to zero. It is quite understandable if one takes into account that the optical atmospheric depth above clouds is appreciably less than that over the clear regions of the Earth's surface.

The influence of cloudiness on the outgoing radiation is not so appreciable in the spectral ranges related to the absorption bands. As should be expected, the difference in the radiation temperatures for the cloudy and cloudless regions in the CO_2 absorption band is small.

A similar effect may be noted for wavelengths longer than 22μ. However, in this case the influence of cloudiness is more appreciable than in the case of CO_2 absorption band. Thus, the joint analysis of spectra of outgoing radiation and cloud distribution allows us to conclude that the cloudiness affects the characteristics of the outgoing radiation of the Earth's surface and atmosphere in all infrared spectrum's ranges to a greater or lesser extent.

Besides, the orbit distribution of radiation temperatures in various spectral ranges and the vertical cross-sections of the temperature in the atmosphere based on the data of aerological soundings were jointly analyzed. The purpose of this analysis was to find the atmospheric layers responsible for the generation of outgoing radiation in one or another spectral range, i. e., to determine the so called effective radiation levels. Orbits close to the synoptical dates were as usually selected for the analysis. It is natural that the determination of the effective levels of radiation in the spectral ranges differing by more or less considerable absirptions is of utmost interest since the effective level for the "transparency window" is none other than the Earth's surface or the cloud surface.

Figure 8 shows an example of the vertical cross-section of temperature in the atmosphere in the plane of orbit 28 (see Fig.7) with the curves of radiation temperature distribution for the wavelengths of 14, 18, 23 and 32μ plotted on it (the numbers of spectra are indicated along the abscissa axis).

It is easy to see that the variations in altitude of the effective radiation level depend on the degree of radiation absorption in the atmosphere in either spectral range. Thus, for 18μ wavelength (rather "transparent" spectral range) these variations cover practically the whole troposphere. They are much smaller for the remainder of wavelengths and they refer only to the upper troposphere; the effective radiation level fluctuates for 14μ from 5 to 8-km, for 23μ from 4 to 8 km and for 32μ from 5 to 11 km

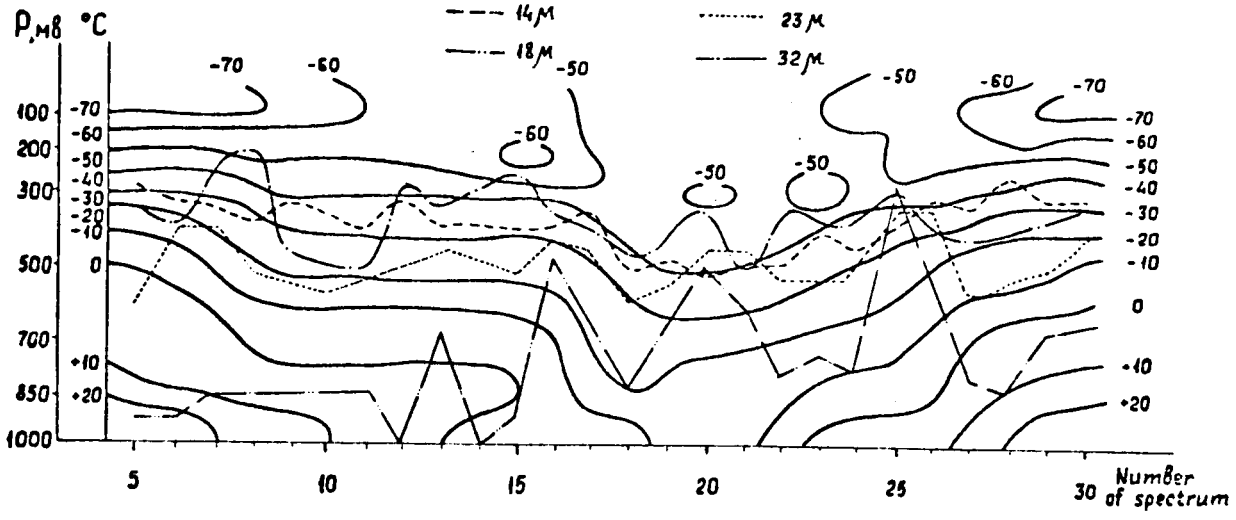

Fig 8

Despite the fact that in these variations the cloud altitude changes are of considerable importance (see Fig.6), it is nevertheless possible to note the latitude dependence of the altitude of the effective level connected with the latitude dependence of moisture content in the atmosphere (decrease of optical atmospheric depth with increasing latitude).

Thus. it has been possible to get an idea about the contribution of various atmospheric layers to the outgoing radiation for various latitude belts.

**** THE END ****

REFERENCES

1. A. I. LEBEDINSKIY, D. N. GLOVATSKIY, V. I. TULUPOV ET AL. The infrared spectroscopy of the Earth's heat radiation." Issl. kosm. prostranstva", Moscow 1965.

2. V. I. ROMANOVSKIY. Matematicheskaya statistika. Tashkent 1961.

3. A. I. LEBEDINSKIY, V. G. BOLGYREV, V. I. TULIPOV ET AL. The spectrum of of the Earth's heat radiation according to observations from COSMOS-45, COSMOS-65 and COSMOS-92 satellites. Space Research VII, cIa, 1966.

CONTRACT No.NAS-5-12487
VOLT TECHNICAL CORPORATION

Prepared by ANDRE L. BRICHANT
on 2 - 4 October 1967
from a preprint X COSPAR.
London 1967